The 15th International Symposium on Magnetic Bearings, August 3-6, 2016, Mojiko Hotel, Kitakyushu, Japan

ISMB15

Analytical Asymmetric Air Gap Model for Active Magnetic Thrust Bearings of Mixed Materials Including Eddy Currents

Robert SEIFERT* and Wilfried HOFMANN*

* Institute of Electrical Power Engineering, Chair of Electrical Machines and Drives, Dresden University of Technology
Helmholtzstraße 9, 01069 Dresden, Germany
E-mail: robert.seifert@tu-dresden.de

Abstract

The electrodynamics of magnetic thrust bearings are characterized by an above-average dependency on the used materials. Axially directed fields render laminated stators and rotors ineffective. High induced voltages inside the magnetic core evoke eddy currents and opposing fields, which are compensated by an additional magnetizing current causing a significant delay between the measurable coil current and the force-related magnetic flux. Although this effect, hampering control dynamics, can be reduced by the use of Soft Magnetic Composites for non-rotating parts, the thrust disk will be made of steel due to its superior tensile strength and saturation flux density. The analytical modeling of mixed-material magnetic thrust bearings reveals new challenges arising from asymmetries and low permeable magnetic core sections, which are both addressed in this paper.

Key words : Active Magnetic Thrust Bearings, Fractional Order Systems, Eddy Currents, Magnetic Levitation Control, Soft Magnetic Composites, Analytical Modeling

1. Introduction

High dynamical active magnetic thrust bearings and actuators are driven by multiples of its rated voltage to achieve high stiffness and force gradients. The underlying rapid flux gradients cause a significant emergence of eddy currents inside the magnetic core. Axially directed fields render laminated stators and rotors ineffective and high induced voltages lead to opposing fields originating from these eddy current loops (Fig. 1a). However, the main flux Φ generating the thrust force F is directly dependent on the terminal voltage u and the opposing fields are compensated by an additional magnetizing current $i'_{\mu\mathrm{Fe}}$. Therefore a significant delay between the measurable coil current and the force-related magnetic flux is observed (Fig. 2). Increasing demand on control dynamics require to overcome these eddy current effects, which in general are characterized by an above-average dependency on the used materials.

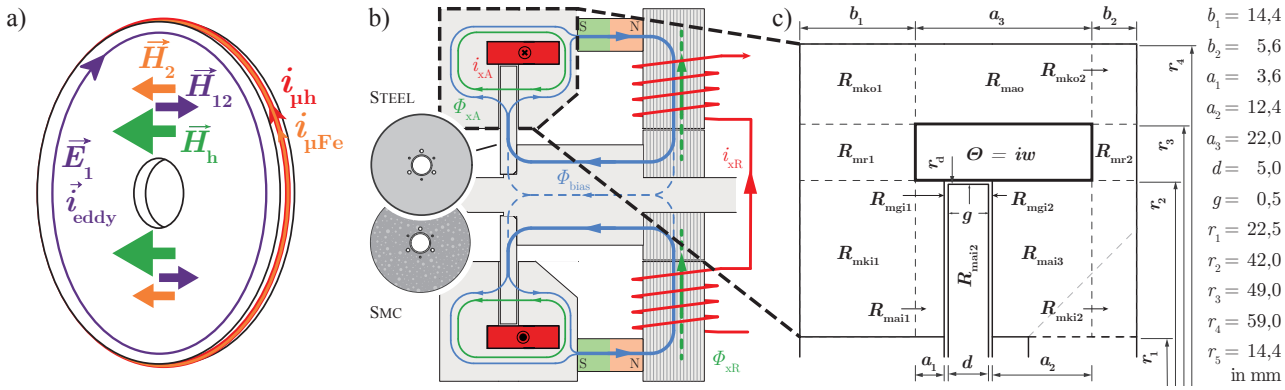

Figure 1 Combined radial/thrust bearing: a) Magnetic fields and eddy current loops in cylindrical core parts, e. g. thrust disk b) Cross section c) Magnetic circuit of thrust bearing divided into effective reluctances.

As a first approach the application of less electrically conductive materials for stator and rotor, like Soft Magnetic Composites (SMC), can reduce the phase delay drastically in comparison to conventional solid steel bearings (Fig. 3). In this case and for laminated radial bearings the eddy current effects can be modeled simply by considering the eddy current time constant T_{Fe} in the equivalent electric circuit as shown in Bahr et al. (2013). But even for bearings partly made of

steel T_{Fe} is generally bigger (up to 10 times for f_{Pulse} = 20 kHz) than the actual inverter pulse width and therefore not applicable, as the state of constant current gradient (section B in Fig. 2) is never reached during one period. However, the lower saturation flux density and weak mechanical strength (σ = 70 MPa) currently disqualify SMC as material especially for the rotating components in industrial high-speed applications.

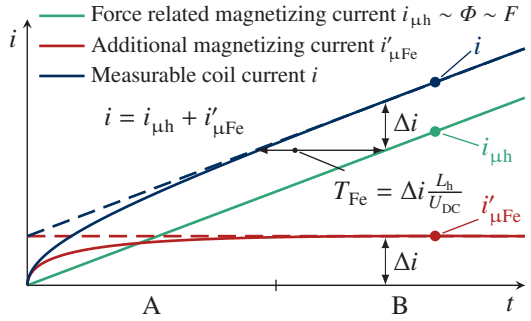

Figure 2 Qualitative currents and its asymptotes immediately after voltage pulse - T_{Fe}: Time delay between measurable coil current and thrust force

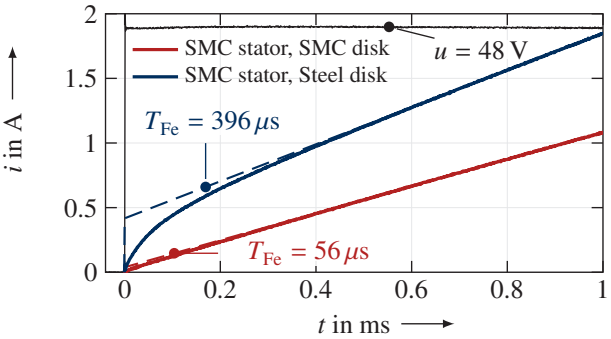

Figure 3 Measured step response of the coil current for 48 V voltage step: comparison of thrust bearing with solid SMC stator and either steel or SMC disk

A second approach is the analytical modeling of the axial magnetic circuit in terms of a reluctance network by solving the underlying differential equations considering the eddy current effects due to the typical high flux gradients. By sufficient simplification of the model a compensation of the main flux delay within the closed-loop control is theoretically possible. Instead of the coil current, the control of the magnetic flux density respectively the force generating magnetizing current is intended. The analytical models of the current and position plants can serve as estimators for the determination of the actual value for the force related air gap flux density B_g from the measured coil current (Fig. 4a). Their transfer functions are based on fractional order systems (Monje et al., 2010) or implicit systems (Riu et al., 2003), a research field still in its early stages. The required approximations of the reluctance network and its practical implementation are the focus of further studies.

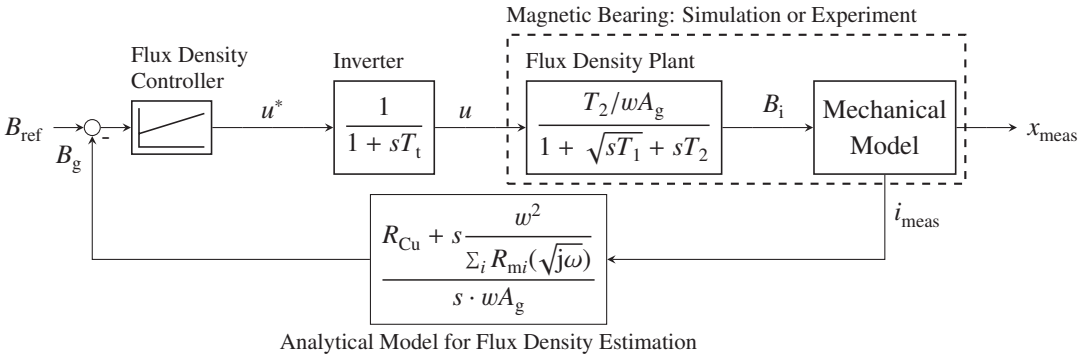

Figure 4 Flux density control loop with measurement of coil current, flux density estimation with fractional order (implicit) system, PID-contoller and fractional-order plant. Parameters: T_2 - main field time constant, T_1 - half order eddy current time constant, T_t - inverter delay, w - number of turns, A_g - area of air gap

In order to achieve low losses, as required e. g. in vacuum applications, and high dynamics a combination of both approaches can be applied as in the studied configuration (Fig. 1). Profiting from the low electrical conductivity and therefore low eddy current density the stator is made of SMC, while for the thrust disk conventional steel (42CrMo4, SAE4140) is used due to its superior tensile strength (σ = 1 GPa). Even though the air gap geometry is still symmetrical, the magnetic field on the steel side of the air gap suffers from a much higher field displacement and the field distribution is asymmetrical. Therefore the assumption of symmetry and identical materials on both sides of the air gap as proposed in previous works (firstly Zhu, 2005; later Sun et al., 2009 and Zhu et al., 2010) is invalid for the employed configuration. This paper focuses on the refinement of the analytical air gap model, contained in the effective air gap reluctance $R_{mgi}(j\omega)$, also for the underlying *asymmetrical case*. Furthermore the reluctances of the stator corners (R_{mk} in Fig. 1c) were usually neglected rightly to date, but the comparatively low relative permeability of SMC recommends their inclusion, as proposed in this paper. Saturation and frequency dependent leakage fluxes are still neglected though and their consideration will be part of future works. The results are validated by FE-analyses.

2. Advanced Magnetic Circuit Model

The electric conductivity κ of the utilized steel grade 42CrMo4 is a thousandfold bigger in comparison to SMC (Somaloy Prototyping Material) causing high eddy currents, which have a great impact on the field distribution within the magnetic core, described by the skin depth δ_α. Hence the analytical model is derived from the diffusion equation, which can be solved for every section (Fig. 1c) of the magnetic core assuming an one-dimensional field propagation, specifically $\vec{B}(\mathbb{R}^3,t) = B(\mathbb{R}^3,t)$ (Stoll, 1974):

$$\Delta B(\mathbb{R}^3,t) = \kappa\mu_0\mu_\mathrm{r}\frac{\mathrm{d}}{\mathrm{d}t}B(\mathbb{R}^3,t) \qquad (1)$$

The geometric derivation indicated by the Laplace operator Δ is independent of the time derivation and Eq. (1) can be rewritten for sinusoidally excitation, assuming an initially constant frequency ω:

$$\Delta\underline{B}(\mathbb{R}^3) = \mathrm{j}\omega\kappa\mu_0\mu_\mathrm{r}\underline{B}(\mathbb{R}^3) = \alpha^2\underline{B}(\mathbb{R}^3) \qquad (2)$$

which has the form of e. g. the *modified Bessel's equation*

$$\frac{\partial^2\underline{B}_z(r)}{\partial r^2} + \frac{1}{r}\frac{\partial\underline{B}_z(r)}{\partial r} - \alpha^2\underline{B}_z(r) = 0\,, \qquad (3)$$

in case of axially permeated cylindrical geometries. In general the solution of the diffusion equation for any magnetic actuator is a function of the *wave propagation constant* α (Kucera et al., 1996) containing the square root of the *complex frequency* $\mathrm{j}\omega$. By integration one can obtain the magnetic flux Φ and the so-called *effective reluctance* R_meff (Tab. 1 - Zhu, 2005; respectively *effective permeability* μ_reff introduced by Rabinovici et al., 1992). A special case reveals the air gap field: though there are no eddy currents, it is not homogeneous as its width is usually to small (Fig. 5). The only partial homogenization was first considered by Zhu (2005) by applying a reluctance network on the air gap.

Table 1 Analytical solutions of all partial reluctances for magnetic cores of a single material (Zhu et al., 2005)

R_{mi}	Formula
R_mai	$\frac{a\cdot\alpha}{2\pi\mu_0\mu_\mathrm{r}r_2}\frac{\mathrm{I}_0^*(r_2\alpha)\,\mathrm{K}_1(r_1\alpha)+\mathrm{I}_1(r_1\alpha)\,\mathrm{K}_0(r_2\alpha)}{\mathrm{I}_1(r_2\alpha)\,\mathrm{K}_1(r_1\alpha)-\mathrm{I}_1(r_1\alpha)\,\mathrm{K}_1(r_2\alpha)}$
R_mao	$\frac{a\cdot\alpha}{2\pi\mu_0\mu_\mathrm{r}r_3}\frac{\mathrm{I}_0(r_3\alpha)\,\mathrm{K}_1(r_4\alpha)+\mathrm{I}_1(r_4\alpha)\,\mathrm{K}_0(r_3\alpha)}{\mathrm{I}_1(r_4\alpha)\,\mathrm{K}_1(r_3\alpha)-\mathrm{I}_1(r_3\alpha)\,\mathrm{K}_1(r_4\alpha)}$
R_mr	$\frac{\ln\frac{r_3}{r_2}}{2\pi\mu_0\mu_\mathrm{r}b}\cdot\frac{b\cdot\alpha}{\tanh(b\cdot\alpha)}$
R_mgi	$\frac{g\cdot\beta}{2\pi\mu_0 r_2}\frac{\mathrm{I}_0(r_2\beta)\,\mathrm{K}_1(r_1\beta)+\mathrm{I}_1(r_1\beta)\,\mathrm{K}_0(r_2\beta)}{\mathrm{I}_1(r_2\beta)\,\mathrm{K}_1(r_1\beta)-\mathrm{I}_1(r_1\beta)\,\mathrm{K}_1(r_2\beta)}$
	with: $\alpha=\sqrt{\mathrm{j}\omega\kappa\mu_0\mu_\mathrm{r}}=\delta_\alpha^{-1}\cdot\sqrt{2\mathrm{j}}\,,\quad\beta=\sqrt{\frac{2\alpha}{g\mu_\mathrm{r}}}$
	*I_ν, K_ν : modified Bessel functions, 1. kind, ν-th order

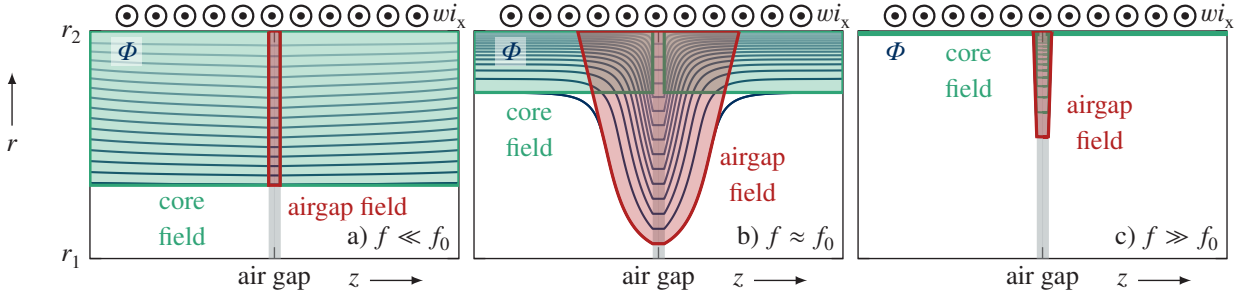

Figure 5 Flux lines Φ within the skin depth δ_α inside a cylindrical iron core with air gap surrounded by a solenoidal excitation coil (wi_x = current linkage) for frequencies a) below, b) around and c) above the threshold frequency f_0 of $R_\mathrm{mg}(\mathrm{j}\omega)$.

He stated that all flux lines in the air gap field region would be either parallel to the air gap surface inside the core or perpendicular through the air gap, which is true for frequencies over a certain material-dependent threshold frequency f_0 (Fig. 5c). It was also assumed that the frequency-dependent width of the air gap field region would not overlap with the adjacent core field region. As shown in Fig. 5b this is not the case for frequencies around f_0, but the error made was found to be negligible by Seifert (2014). The modeling of the air gap field region with a reluctance network is thoroughly discussed in Zhu et al. (2005) and leads to the air gap reluctance R_mgi (Eq. (4)). For low frequencies (Fig. 5a) the air gap field is nearly homogeneous as expected, confirmed by the convergence of $R_\mathrm{mgi}(\mathrm{j}\omega)$ to its stationary value for $\omega\to 0$.

$$R_\mathrm{mgi}(\mathrm{j}\omega) = \frac{g\cdot\beta}{2\pi\mu_0 r_2}\frac{\mathrm{I}_0(r_2\beta)\,\mathrm{K}_1(r_1\beta)+\mathrm{I}_1(r_1\beta)\,\mathrm{K}_0(r_2\beta)}{\mathrm{I}_1(r_2\beta)\,\mathrm{K}_1(r_1\beta)-\mathrm{I}_1(r_1\beta)\,\mathrm{K}_1(r_2\beta)} \quad\text{with}\quad \beta=\sqrt{\frac{2\alpha(\mathrm{j}\omega)}{g\mu_\mathrm{r}}},\quad \mathrm{I}_\nu,\mathrm{K}_\nu:\ \text{modified Besselfunctions} \qquad (4)$$

However, Zhu's solution assumes identical materials on both sides of the air gap. In consequence he solely defines the *air gap wave propagation constant* β for a *single* material. This paper proposes an approach to determine the *asymmetrical air gap wave propagation constant* β_{12} which firstly covers the case of *mixed* materials within a magnetic circuit (Sec. 2.1).

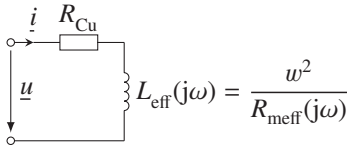

Figure 6 Equivalent circuit of magnetic thrust bearing with effective inductance

Assuming a single core material and ignoring the corner elements R_{mk}, all reluctances found by Zhu (Tab. 1) can be summed up to form an electric circuit (Fig. 6) with the *effective inductance* L_{eff} with the number of turns w.

$$\Rightarrow \quad \frac{i(\mathrm{j}\omega)}{u(\mathrm{j}\omega)} = \frac{1}{R_{Cu} + \mathrm{j}\omega L_{eff}} = \frac{1}{R_{Cu} + \mathrm{j}\omega \dfrac{w^2}{\sum\limits_i R_{mi}(\mathrm{j}\omega)}} \,. \tag{5}$$

2.1. Air Gap Model Considering Asymmetrical Air Gap Field Distribution

Though the current density within the air gap is $J = 0$, an inhomogeneous air gap field implies an *air gap skin depth* δ_β. It corresponds to the skin depth of the current density field at the boundary surface between core and air gap field. In case there are different materials (characterized by α_1 and α_2 and respectively β_1 and β_2) on both sides of the air gap, there obviously exists an *asymmetrical air gap wave propagation constant* β_{12} in-between β_1 and β_2.

The main elements of the magnetic thrust bearing (Fig. 1c) are solid hollow cylinders (R_{mai}, R_{mao}) permeated by an axially directed flux density field $\vec{B}$, changing its direction analogous to the frequency ω of its provoking harmonic magnetizing current i. According to Lenz's law a delayed circular current density field $\vec{J}$ is evoked by the change of $\vec{B}$ forming an oscillating electromagnetic wave. For high frequencies ω the J-field can only follow the oscillation close to the surface of the magnetic conductor, which is called the *skin effect* characterized by the *core skin depth* δ_α. Within δ_α the current density wave is moving with the propagation speed $v = \omega \cdot \delta_\alpha$. At the boundary between two materials the propagation speed is changing due to the differences in permeability μ and conductivity κ of the materials. However the change is not stepwise as the continuity condition of the normal component of the flux density $\vec{n} \cdot (B_{n1} - B_{n2}) = 0$ would be violated. At a certain point at the boundary $[r = x_{12},\ z = 0]$ therefore applies $B_{n1} = B_{n2}$, which also requires the propagation speeds v_1 and v_2 to adopt a mean value v_{12}. The mean value v_{12} of speeds in respective to a fixed displacement x_{12} - and hence the proportional skin depth $\delta_{\alpha 12}$ - are generally calculated by the *harmonic mean*:

$$\frac{1}{v_{12}} = \frac{1}{2}\left(\frac{1}{v_1} + \frac{1}{v_2}\right) \quad \overset{v \sim \delta_\alpha}{\Longrightarrow} \quad \frac{1}{\delta_{\alpha 12}} = \frac{1}{2}\left(\frac{1}{\delta_{\alpha 1}} + \frac{1}{\delta_{\alpha 2}}\right) \quad \text{at the boundary} \quad z = 0 \,. \tag{6}$$

This relationship was verified by FE-analyses in Seifert, 2014. For the wave propagation constant α, being the reciprocal of δ_α, follows the *arithmetic mean*:

$$\alpha = \frac{\sqrt{2\mathrm{j}}}{\delta_\alpha} \quad \Longrightarrow \quad \alpha_{12} = \frac{1}{2}(\alpha_1 + \alpha_2) \,. \tag{7}$$

In the most cases in conjunction with magnetic actuators and bearings the direct boundary between two core materials is not of interest, but the transition between two materials bridging an air gap, like in the underlying case of a magnetic thrust bearing consisting of a SMC stator paired with a steel thrust disk. It can be assumed that the flux takes the shortest path over the air gap between both stator paths. Consequently it flows ideally in axial direction and the normal component of the flux density B_n is constant. Therefore one can assume, that above relations remain valid in spite of the air gap. By

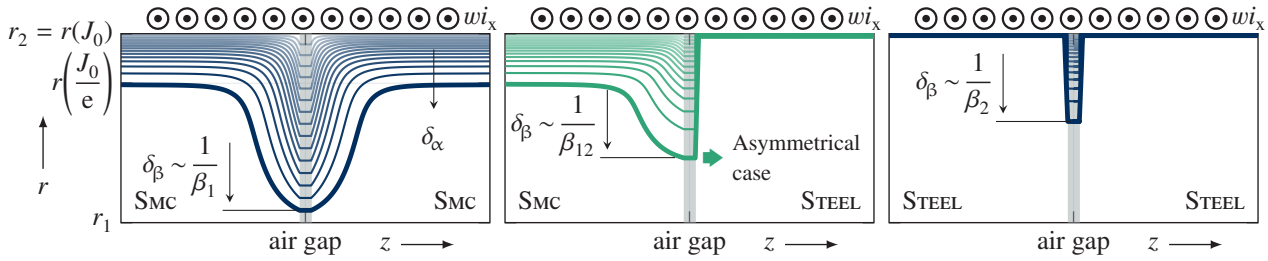

Figure 7 Exemplary eddy current density J inside a cylindrical iron core (of different material combinations: $\kappa_{SMC} \ll \kappa_{Steel}$) with air gap surrounded by a solenoidal excitation coil (w = number of turns, current i_x of arbitrary frequency). *Skin depth* δ: particular radius where current density falls to 37 % of its surface value: $\delta(z) = r(z, J = \mathrm{e}^{-1} J_0)$. *Core skin depth* δ_α: equal for each material in all three cases. *Air gap skin depth*: δ_β depends on both materials.

calculating the air gap wave propagation constant β by its known formula (Tab. 1) and inserting it into Eq. (7) it becomes apparent that indeed the air gap g is canceled out and β_{12} persists independent of it:

$$\beta = \sqrt{\frac{2\alpha}{g\mu_r}} \quad \Rightarrow \quad \alpha = \frac{\beta^2 \cdot g\mu_r}{2} \quad \overset{\text{into Eq. (7)}}{\Longrightarrow} \quad \beta_{12}^2 \mu_{r12} = \frac{1}{2}\left(\beta_1^2 \mu_{r1} + \beta_2^2 \mu_{r2}\right) \,. \tag{8}$$

Furthermore an analysis of the unit of the air gap propagation constant $[\beta] = 1/\mathrm{m}$ suggests the relation

$$\beta \sim \frac{1}{\delta_\beta} \quad \text{and therefore} \quad \delta_\beta \sim \sqrt[4]{\frac{\mu}{\kappa}} \quad \text{and} \quad \delta_\beta = \frac{c}{\beta} \quad \text{with} \quad c = \sqrt[8]{-2}\,. \tag{9}$$

The novel definition of the proportionality constant c was found empirical by FE-analysis (e. g. Fig. 8, Seifert, 2014) with no mathematical proof yet, but appears to be exact for high frequencies leading to the case in Fig. 5c, matching the general validity of the reluctance model.

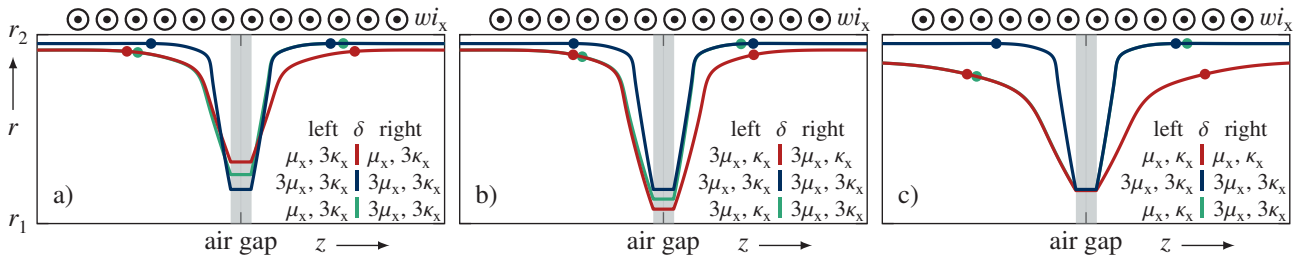

Figure 8 Skin depth of current density ($\delta = r(J = J_0/\mathrm{e}) \Rightarrow$ contour line $J = J_0/\mathrm{e} = J(r_2)/\mathrm{e}$) in stator and air gap ($g = 0.5\,\mathrm{mm}$) for an arbitrary frequency f_x, permeability μ_x and conductivity κ_x where it applies $\delta_\alpha \sim \sqrt{\mu\kappa}$ and $\delta_\beta \sim \sqrt[4]{\mu/\kappa}$
a) if $\kappa = \text{const.} \Rightarrow \delta_\alpha = f(1/\mu), \delta_\beta = f(\mu)$ b) if $\mu = \text{const.} \Rightarrow \delta_\alpha = f(1/\kappa), \delta_\beta = f(1/\kappa)$ c) if $\mu/\kappa = \text{const.} \Rightarrow \delta_\beta = \text{const.}$

The *average permeability* μ_{r12} is a mathematical auxiliary quantity which can be calculated recursively from the special case in Fig. 8c. It becomes apparent that no matter how much the core skin depths $\delta_{\alpha 1}$ and $\delta_{\alpha 2}$ diverge, the air gap skin depth δ_β is equal for any material combination as long as the proportion μ/κ is equal for both materials, which can be used as boundary condition

$$\delta_{\beta 1} = \delta_{\beta 2} = \delta_{\beta 12} \implies \frac{c}{\beta_1} = \frac{c}{\beta_2} = \frac{c}{\beta_{12}} \implies \beta_{12}^2 = \beta_1^2 = \beta_2^2 = \beta^2 \tag{10}$$

to obtain the solution for μ_{r12} from Eq. (8), leading to the arithmetic mean of μ_{r1} and μ_{r2}:

$$\beta^2 \mu_{r12} = \frac{1}{2}\left(\beta^2 \mu_{r1} + \beta^2 \mu_{r2}\right) \implies \mu_{r12} = \frac{1}{2}\left(\mu_{r1} + \mu_{r2}\right) \tag{11}$$

Finally for the *asymmetrical air gap wave propagation constant* β_{12} and *asymmetrical air gap skin depth* β_{12} can be stated

$$\beta_{12} = \sqrt{\frac{2 \cdot \alpha_{12}}{g \cdot \mu_{r12}}} = \sqrt{\frac{2 \cdot (\alpha_1 + \alpha_2)}{g \cdot (\mu_{r1} + \mu_{r2})}} = \sqrt{\frac{\beta_1^2 \cdot \mu_{r1} + \beta_2^2 \cdot \mu_{r2}}{\mu_{r1} + \mu_{r2}}} \quad \text{and} \quad \frac{\mu_{r1} + \mu_{r2}}{\delta_{\beta 12}^2} = \frac{1}{2}\left(\frac{\mu_{r1}}{\delta_{\beta 1}^2} + \frac{\mu_{r2}}{\delta_{\beta 2}^2}\right). \tag{12}$$

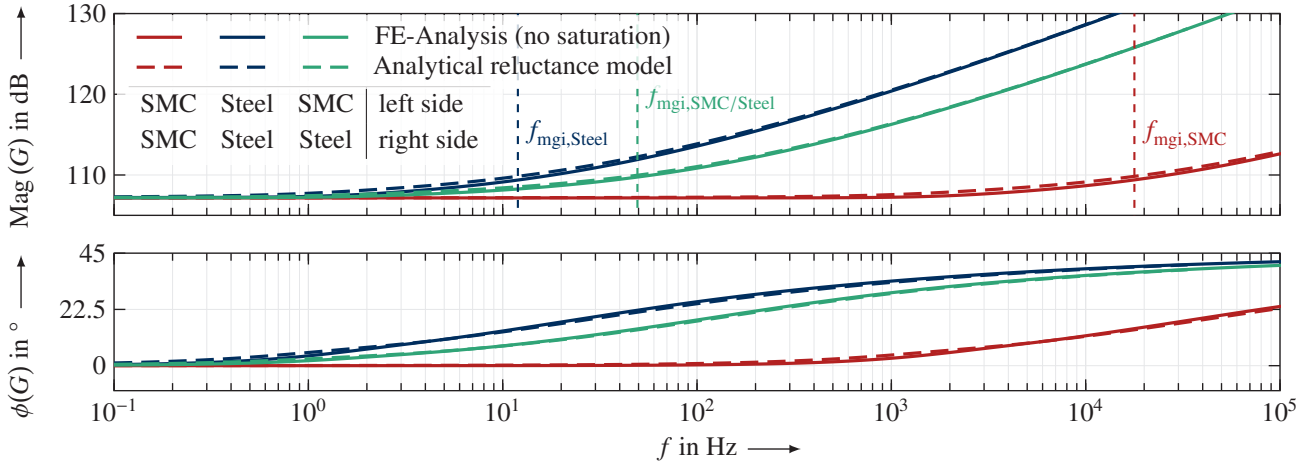

Figure 9 Bode plot of the effective air gap reluctance and adjacent axial core reluctances $G(\mathrm{j}\omega) = R_{mgi}(\mathrm{j}\omega) + 2 \cdot R_{mai}(\mathrm{j}\omega)$ for the three cases and exemplary geometry of Fig. 7: $a_1 = a_2 = 11\,\mathrm{mm}$, $r_1 = 22.5\,\mathrm{mm}$, $r_2 = 42\,\mathrm{mm}$, $g = 0.5\,\mathrm{mm}$, f_{mgi}: threshold frequencies of air gap reluctances R_{mgi}

Figure 9 shows that the reluctance R_{mgi} for the asymmetric case fits well in-between the symmetric cases. The maximum error compared to the FE-analysis is only 4 % for the latter and 2 % for the first case. It arises due to the overlapping of R_{mgi} and R_{mai} close to the respective threshold frequencies as explained in Fig. 5. Obviously for the asymmetric case the error is halved, as the overlapping just occurs on one side of the air gap for a certain frequency.

2.2. Consideration of corner reluctances

The corner reluctances R_{mk} (Fig. 1c) were usually neglected (Zhu et al., 2005; Sun et al., 2009) because of their low impact in case of high permeable steel cores. But for SMC stators ($\mu_r < 600$) their disregard will cause an error of up to 7 % of the stationary value of the total effective reluctance R_{meff}, which recommends their inclusion. Due to the appearance of elliptic integrals there is no analytical field solution of the diffusion equation (2) for this geometry and other approaches (Flax et al., 1966) are too extensive to be used in this case. However, FE-analyses have shown that the determination of the stationary value ($f = 0$) of R_{mk} is sufficient. Indeed the effective reluctance would rise for high frequencies owing to the skin effect, but on the other hand the flux path becomes shorter so as to both effects are canceled out for common corner geometries. In Seifert (2014) is thoroughly derived how the corners of the magnetic core can be approximated by a toroid with an quarter-elliptic cross-section (Fig. 10) resulting in Eq. (13)

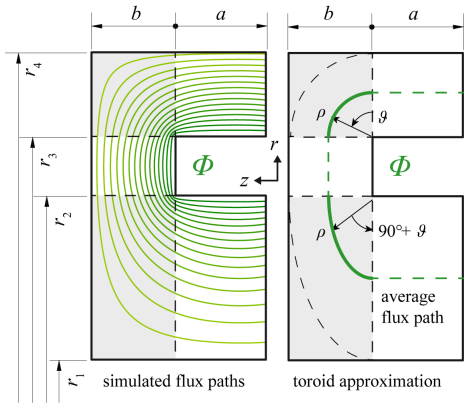

Figure 10 Simulated flux lines for low frequencies and assumptions for the approximation of the stator corners with a toroid

$$R_{mki0} = \sum_{n=1}^{N} \left[\frac{0.72/\pi\mu_0\mu_r}{\sqrt{4r_2^2 - \rho_n^2}} \tan^{-1} \frac{(2r - \rho_n) \cdot \tan\left(\frac{\pi\theta}{4}\right)}{\sqrt{4r_2^2 - \rho_n^2}} \right]_{1+\frac{n-1}{N}}^{1+\frac{n}{N}}$$

$$\text{with } \rho_n = \sqrt{b^2 \sin^2\theta_n + r_2^2 \cos^2\theta_n},\ \theta_n = \frac{\pi}{2}\left(1 + \frac{n - \frac{1}{2}}{N}\right) \quad (13)$$

for the lower corners and Eq. (14) for the upper corners:

$$R_{mko0} = \sum_{n=1}^{N} \left[\frac{0.72/\pi\mu_0\mu_r}{\sqrt{4r_3^2 - \rho_n^2}} \tan^{-1} \frac{(2r - \rho_n) \cdot \tan\left(\frac{\pi\theta}{4}\right)}{\sqrt{4r_3^2 - \rho_n^2}} \right]_{\frac{n-1}{N}}^{\frac{n}{N}}$$

$$\text{with } \rho_n = \sqrt{b^2 \sin^2\theta_n + r_3^2 \cos^2\theta_n},\ \theta_n = \frac{\pi}{2}\left(\frac{n - \frac{1}{2}}{N}\right). \quad (14)$$

The arithmetic series (13, 14) converge and the limit can be approximated numerically with a sufficiently large N.

3. Conclusion and outlook

Together with the firstly considered reluctances of the stator corners R_{mk} and the improvement of the air gap reluctance network by Zhu et al. leading to R_{mgi}, in this paper the established models are completed for use with any cylindrical magnetic actuator and active magnetic thrust bearings designed with mixed materials. Over a wide frequency range the reluctance model agrees well with the FE-analysis (Fig. 11) and there occur only minor deviations due to the unavoidable overlapping of part reluctances.

A major deficiency of the current state is the non-consideration of saturation. Although low saturation can be easily achieved for magnetic thrust bearings by design, the skin effect drives the surface - especially of the steel made thrust disk - into saturation, which also causes the main flux to gap the thrust disk on the whole. Both effects are highly frequency dependent and correlated, what makes them challenging to consider. Sun et al. (2009) already expanded the reluctance network of Zhu et al. (2005) by parallel leakage reluctances, which can be included into this model as a next step.

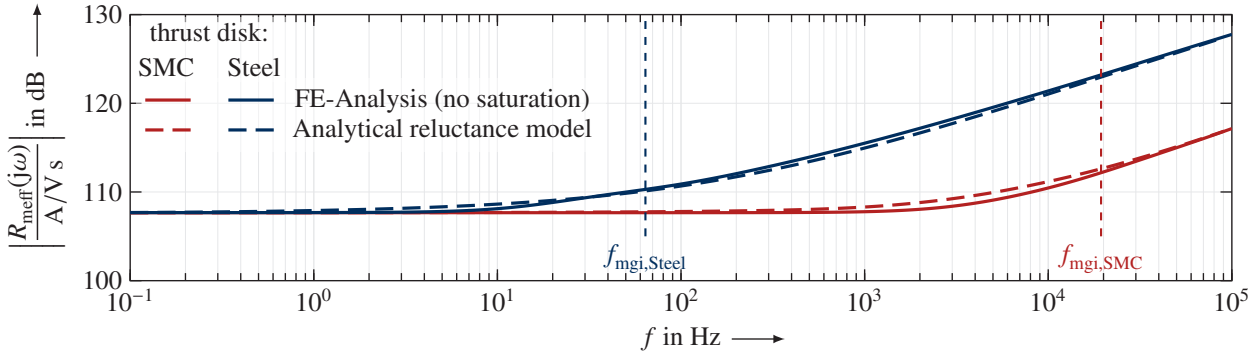

Figure 11 Magnitude plot of the total effective reluctance R_{meff} of the magnetic circuit, FE-analysis with neglected saturation and analytical solution, f_{mgi}: threshold frequency of air gap reluctance R_{mgi}

Having a closer look at the frequency response of the characteristically total effective reluctance $R_{\mathrm{meff}}(\mathrm{j}\omega)$ (Fig. 11) it reveals an unusual gradient of 10 dB/decade for high frequencies, indicating a *half-order system* $G(s^{1/2})$, which was expectable as all reluctances $R_{\mathrm{m}i}$ in Tab. 1 are proportional to the wave propagation constant α and the square root of the complex frequency $\sqrt{\mathrm{j}\omega}$. Our further research is aimed at showing how *fractional-order* systems, controllers and estimators can be used for a high dynamic magnet bearing control.

4. Acknowledgment

The authors would like to thank F. Bahr for his valuable input on the final manuscript and the German Research Foundation (DFG) for funding this project under the grant HO 1483/64-1.

References

Bahr, F. et al. (2013). "Permanent Magnet Bias AMB Using Integrated Hall Sensor Based Air Gap Flux Density Feedback". In: *Brazilian Workshop on Magnetic Bearings*.

Flax, L. and J. H. Simmons (1966). *Magnetic field outside perfect rectangular conductors*. Tech. rep. NASA.

Kucera, L. and M. Ahrens (1996). "A simple dynamic model for eddy currents in a magnetic actuator". In: *Third International Symposium on Magnetic Suspension Technology*.

Monje, C. et al. (2010). *Fractional-order Systems and Controls: Fundamentals and Applications*. Advances in Industrial Control. London: Springer.

Rabinovici, R. and B. Kaplan (1992). "Effective magnetization and forces due to eddy currents". In: *IEEE Transactions on Magnetics* 28.3, pp. 1863–1869.

Riu, D. M., N. M. Retiere, and M. S. Ivanes (2003). "Induced currents modeling by half-order systems application to hydro- and turbo-alternators". In: *IEEE Transactions on Energy Conversion* 18.1, pp. 94–99.

Seifert, R. (2014). "Untersuchung der Eisenkreiszeitkonstante eines axialen Magnetlagers (*Investigation on the eddy current time constant of a magnetic thrust bearing*)". German. Diplomarbeit/MSc Thesis. Dresden University of Technology.

Stoll, R. (1974). *The analysis of eddy currents*. Monographs in electrical and electronic engineering. Oxford: Clarendon Press.

Sun, Y., Y.-S. Ho, and L. Yu (2009). "Dynamic Stiffnesses of Active Magnetic Thrust Bearing Including Eddy-Current Effects". In: *IEEE Transactions on Magnetics* 45.1, pp. 139–149.

Zhu, L. (2005). "Non-laminated Magnetic Actuators: Modeling and Performance Limitations". PhD thesis. University of Virginia.

Zhu, L. and C. Knospe (2010). "Modeling of Nonlaminated Electromagnetic Suspension Systems". In: *Mechatronics, IEEE/ASME Transactions on* 15.1, pp. 59–69.

Zhu, L., C. Knospe, and E. H. Maslen (2005). "Analytic model for a nonlaminated cylindrical magnetic actuator including eddy currents". In: *IEEE Transactions on Magnetics* 41.4, pp. 1248–1258.